RHEUMATOLOGY

Original article

doi:10.1093/rheumatology/kex258

Effects of tofacitinib in early arthritis-induced bone loss in an adjuvant-induced arthritis rat model

Bruno Vidal[1], Rita Cascão[1], Mikko A.J. Finnilä[2,3], Inês P. Lopes[1], Vânia G. da Glória[1], Simo Saarakkala[2,4], Peter Zioupos[5], Helena Canhão[6] and João Eurico Fonseca[1,7]

Abstract

Objectives. The main goal of this work was to analyse how treatment intervention with tofacitinib prevents the early disturbances of bone structure and mechanics in the rat model of adjuvant-induced arthritis. This is the first study to access the impact of tofacitinib on the skeletal bone effects of inflammation.

Methods. Fifty Wistar rats with adjuvant-induced arthritis were randomly housed in experimental groups, as follows: non-arthritic healthy group (n = 20); arthritic non-treated group (n = 20); and 10 animals undergoing tofacitinib treatment. Rats were monitored during 22 days after disease induction for the inflammatory score, ankle perimeter and body weight. Healthy non-arthritic rats were used as controls for comparison. After 22 days of disease progression, rats were killed and bone samples collected for histology, micro-CT, three-point bending and nanoindentation analysis. Blood samples were also collected for quantification of bone turnover markers and systemic cytokines.

Results. At the tissue level, measured by nanoindentation, tofacitinib increased bone cortical and trabecular hardness. However, micro-CT and three-point bending tests revealed that tofacitinib did not reverse the effects of arthritis on the cortical and trabecular bone structure and on mechanical properties.

Conclusion. Possible reasons for these observations might be related to the mechanism of action of tofacitinib, which leads to direct interactions with bone metabolism, and/or to the kinetics of its bone effects, which might need longer exposure.

Key words: rheumatoid arthritis, bone, inflammation, DMARD, animal models

BASIC SCIENCE

Rheumatology key messages

- Tofacitinib was able to control inflammatory activity in an adjuvant-induced arthritis rat model.
- Tofacitinib increased bone hardness but did not reverse structural and mechanical bone fragility induced by arthritis.

Introduction

RA is a chronic immune-mediated inflammatory disease, which affects ~1% of the world population [1]. RA is associated with an increased expression of the RANK ligand (RANKL) and low levels of its antagonist, osteoprotegerin (OPG) [2]. RANKL is a crucial activator of osteoclastogenesis [3]. In addition, RA serum and synovial fluid (SF) present an inflammatory cytokine profile, including IL-1β, IL-6, IL-17 and TNF, which further favours osteoclast differentiation and activation, starting in the early phase of the disease [4–6]. Evidence suggests that an imbalance in bone remodelling in RA contributes not only to local bone erosions but also to the development of systemic

[1]Instituto de Medicina Molecular, Faculdade de Medicina, Universidade de Lisboa, Lisbon, Portugal, [2]Research Unit of Medical Imaging, Physics and Technology, Faculty of Medicine, University of Oulu, Oulu, [3]Department of Applied Physics, University of Eastern Finland, Kuopio, [4]Medical Research Center, University of Oulu, Oulu, Finland, [5]Biomechanics Laboratories, Cranfield Forensic Institute, Cranfield University, Defence Academy of the UK, Shrivenham, UK, [6]CEDOC, EpiDoC Unit, NOVA Medical School and National School of Public Health, Universidade Nova de Lisboa, Lisboa, Portugal and [7]Rheumatology Department, Centro Hospitalar de Lisboa Norte, EPE, Hospital de Santa Maria, Lisbon Academic Medical Centre, Lisbon, Portugal

Submitted 11 October 2016; revised version accepted 5 June 2017

Correspondence to: Bruno Vidal, Instituto de Medicina Molecular, Faculdade de Medicina da Universidade de Lisboa, Av. Professor Egas Moniz, 1649-028 Lisboa, Portugal.
E-mail: vidal.bmc@gmail.com

osteoporosis [7] and increased rates of vertebral and hip fractures in these patients [8, 9].

Tofacitinib is a selective inhibitor of Janus kinase 1 (JAK1) and Janus kinase 3 (JAK 3), thus interfering with the dimerization of signal transducer and activator of transcription (STAT) molecules, blocking the activation of gene transcription that is dependent on the JAK–STAT signalling pathway [10–12]. Tofacitinib has been recently approved by the European Medicines Agency for the indication of RA treatment [13]. The main goal of this work was to analyse whether treatment intervention with tofacitinib in the rat model of adjuvant-induced arthritis (AIA) prevents the early disturbances of bone structure and strength induced by inflammation.

Methods

Animals and experimental design

Fifty 8-week-old female Wistar AIA rats weighing ~200 g were housed in European type II standard filter top cages (Tecniplast, Buguggiate, Italy) and transferred into the specific pathogen-free animal facility at the Instituto de Medicina Molecular, Lisboa, Portugal. The AIA rats were purchased from Charles River Laboratories international (Barcelona, Spain).

Sample size was calculated using the Power Analysis statistical test from the G*Power 3.1 software [14]. The test was based on our own previous data [15], comparing the medians of the experimental groups using the Mann–Whitney *U*-test, with α (probability of error) = 0.05, power = 95%, effect size = 1.751632 and actual power = 0.95072 [16].

Upon arrival, animals were individually identified and randomly housed in experimental groups, as follows: non-arthritic healthy group (n = 20); arthritic rats treated with tofacitinib (10 mg/kg body weight, by oral gavage, twice a week; n = 10); and arthritic rats not treated (received an equal volume of vehicle, 0.5% methylcellulose in water; n = 20). Tofacitinib administration was started 4 days after disease induction, when animals already presented clinical signs of arthritis. The inflammatory score, ankle perimeter and body weight were measured during the period of treatment. Inflammatory signs were evaluated by counting the score of each joint on a scale of 0–3 (0: absence; 1: erythema; 2: erythema and swelling; 3: deformities and functional impairment). The total score of each animal was defined as the sum of the partial scores of each affected joint. Rats were killed 22 days after induction of disease, because maximal disease activity and severity occurs at day 19, plateaus up to day 22 after disease induction, and thereafter the inflammatory signs disappear [17]. Blood, paws and bone samples were collected.

Experiments were approved by the Animal User and Ethical Committees, at the Instituto de Medicina Molecular (Lisbon University), according to Portuguese law and European recommendations.

Histological evaluation of hind paws

Left hind paw samples collected at the time of sacrifice were fixed immediately in 10% neutral buffered formalin solution and then decalcified in 10% formic acid. Samples were then dehydrated, embedded in paraffin, and serially sectioned at a thickness of 5 μm. Sections were stained with Haematoxylin and Eosin for histopathological evaluation of structural changes and cellular infiltration. This evaluation was performed in a blinded fashion using five semi-quantitative scores, as follows: sublining layer infiltration score (0: none to diffuse infiltration; 1: lymphoid cell aggregate; 2: lymphoid follicles; 3: lymphoid follicles with germinal centre formation); lining layer cell number score (0: fewer than three layers; 1: three to four layers; 2: five to six layers; 3: more than six layers); bone erosion score (0: no erosions; 1: minimal; 2: mild; 3: moderate; 4: severe); cartilage surface (0: normal; 1: irregular; 2: clefts; 3: clefts to bone); and global severity score (0: no signs of inflammation; 1: mild; 2: moderate; 3: severe).[18]

Immunohistochemical staining of osteocalcin-positive cells in hind paws

Immunolocalization of osteoblasts was performed by staining with osteocalcin primary antibody (Abcam, Cambridge, UK) followed by EnVision+ (Dako, Glostrup, Denmark). Colour was developed by a solution containing diaminobenzadine tetrahydrochloride (Sigma, Missouri, USA), 0.5% H_2O_2 in phosphate buffer. Slides were counterstained with Haematoxylin and mounted. Immunohistochemical evaluation of rat joints was performed in a blinded fashion using a semi-quantitative score of 0–3 (0: 0–25% staining; 1: 26–50% staining; 2: 51–75% staining; 3: >75% staining) [19]. Histological and imunohistochemical images were acquired using a Leica DM2500 microscope (Leica Microsystems, Wetzlar, Germany) equipped with a colour camera.

STAT1 and suppressor of cytokine signalling 1 expression in bone

Expression of STAT1 and suppressor of cytokine signalling 1 (SOCS1) was quantified by quantitative PCR in bone tissue (tibia) from untreated (n = 14) and tofacitinib-treated rats (n = 10). Tibiae were collected after the rats were killed and stored at −80 °C. On top of dry ice, each frozen tibia was quickly pulverized with a mortar and pestle, which was previously cooled with liquid nitrogen to maintain a very low temperature and prevent RNA degradation. After pulverization, 2 ml of Trizol reagent (Invitrogen, Carlsbad, CA, USA) was added to the powder, preformed following the manufacturer's instructions.

For quantitative PCR analysis, 1.5 μg of RNA from the tibia was treated with DNase I (Roche, Pleasanton, CA, USA) and reversed transcribed using NZY First-Strand cDNA Synthesis Kit (nzytech, Lisboa, Portugal) with random hexamer oligos. Real-time quantitative PCR was performed with Power SYBR® Green PCR Master Mix (Applied Biosystems, Foster City, CA, USA) and gene-specific primers for STAT1 (STAT1_F: 5′-TTGACAGTATGATGAGCGCAGT-3′; STAT1_R: 5′-TGAAGGAACAGTAGCAGGAAGG-3′) and SOCS1 (SOCS1_F: 5′-TGGCACGCATCCCTCTTAAC-3′; SOCS1_R: 5′-CACTTAATGCTGCGGGCAC-3′). PCR was performed in a ViiA™ 7 Real-Time PCR System (Applied Biosytems,

Foster City, CA, USA), with an initial step at 50°C for 2 min and 95°C for 10 min, followed by 40 cycles at 95°C for 15 s and 60°C for 1 min. Attachment region binding protein (ARBP) was used as the reference gene (ARBP_F: 5′-TCG AAGCAAAGGAAGAG TCGG-3′; ARBP_R: 5′-AGGCTGACTT GGTGTGAGGG-3′. Cycle threshold (CT) values were acquired, and the $2^{-\Delta CT}$ method was used for analysis.

Quantification of bone remodelling and inflammatory markers

Serum samples were collected at sacrifice and stored at −80 °C. Bone remodelling markers, carboxy-terminal telopeptide of type I collagen (CTX-I) and procollagen type I propeptides (P1NP), were quantified by Serum Rat Laps ELISA assay (Immunodiagnostic Systems Ltd, Boldon, UK).

The pro-inflammatory cytokines IL-1β, IL-6 (Boster Bio, California, USA), IL-17, OPG, RANKL (Sunred Biological Technology, Shangai, China) and TNF (RayBiotech, Georgia, USA) were quantified in serum samples using specific rat ELISA kits.

Standard curves were generated by using reference biomarker concentrations. Samples were analysed using a plate reader (Infinite M200; Tecan, Mannedorf, Switzerland).

Micro-CT analysis

Structural properties of the trabecular and cortical tibiae were determined with a high-resolution micro-CT system (SkyScan 1272; Bruker microCT, Kontich, Belgium). Moist bones were wrapped in parafilm and covered with dental wax to prevent drying and movement during the scanning. The X-ray tube was set to 50 kV, and the beam was filtered with a 0.5 mm aluminium filter. The sample position and camera settings were adjusted to provide a 3.0 μm isotropic pixel size, and projection images were collected every 0.2°. Tissue mineral density values were calibrated against hydroxyapatite phantoms with densities of 250 and 750 mg/cm^3. Reconstructions were done with NRecon (v 1.6.9.8; Bruker micro-CT), where appropriate corrections to reduce beam hardening and ring artefacts were applied. Bone was segmented in slices of 3 μm thickness. After 200 slices from the growth plate, we selected and analysed 1400 slices of trabecular bone. For cortical bone, 300 slices (1800 slices from the growth plate) were analysed.

Analyses were performed in agreement with guidelines for assessment of bone microstructure in rodents using micro-CT [20]. Trabecular bone morphology was analysed by applying global threshold and despeckle to provide binary image for three-dimensional analyses.

Bone mechanical tests

Femurs were subjected to a three-point bending test using a universal materials testing machine (Instron 3366; Instron Corp., Massachusetts, USA). Femurs were placed horizontally, anterior side upward, on a support with span length of 5 mm. The load was applied with a constant speed of 0.005 mm/s until failure occurred. Stiffness was analysed by fitting a first-degree polynomial function to the linear part of the recorded load deformation data. A displacement of 0.15 μm between the fitted slope and the measured curve was used as the criterion for the yield point, whereas the breaking point was defined as set where force reached maximal value. Force, deformation and absorbed energy were defined both at yield and at the breaking point.

Nanoindentation

Nanoindentation was performed using a CSM-Nano Hardness Tester System (Indentation v.3.83; CSM Instruments SA, Peseux, Switzerland) equipped with a Berkovich diamond tip. After micro-CT, 0.5 mm was cut off the top of the tibia, and the proximal part was embedded in low-viscosity epoxy resin (EpoThin; Buehler, Knorring Oy Ab, Helsinki, Finland). A slow-speed diamond saw was used to remove 10% of the bone length. The sample surface was polished using silicon carbide sandpaper with a decreasing grid size (800, 1200, 2400 and 4800) and finished with a cloth containing 0.05 μm γ-alumina particles. The indentation protocol was adopted from previous work [21], and on average, eight indentations were made on both cortical and trabecular bone with a quasi-static loading protocol. All indentations were performed under an optical microscope to achieve the precise location of indentations at the centre of the targeted area in the tissue [22].

A trapezoidal loading waveform was applied with a loading–unloading rate of 20 mN/min and with an intermediate load-hold phase lasting 30 s hold at a maximal load 10 mN. The hardness (H_{IT}), indentation modulus (E_{IT}), indentation creep (C_{IT}) and elastic part of indentation work (η_{IT}) were measured by using the method of Oliver and Pharr (1992) [23].

Histological images of rat tibiae from the diaphyseal cortical region were acquired during the nanoindentation technique.

A histological score was applied in order to evaluate the lamellar structures of bone tissue (lamellar bone structure: 1: predominantly parallel lamellae (PL); 2: concentric and PL in the same proportion; 3: predominantly concentric lamellae).

The ratio of osteocyte lacuna area/total tissue area was also evaluated at ×200 magnification in order to analyse the percentage of the total tissue area occupied by osteocyte lacunae. The acquisition method and analysis used were the same as those applied for the evaluation of bone volume/tissue volume in the histomorphometry technique [15]. All variables were expressed and calculated according to the recommendations of the American Society for Bone and Mineral Research [24], using a morphometric program (Image J 1.46 R with plugin Bone J, Bethesda, Maryland, USA).

Statistical analysis

Statistical differences were determined with the Mann–Whitney U-test using GraphPad Prism (GraphPad, San Diego, CA, USA). Data were expressed as the median with interquartile range. Differences were considered statistically significant for $P < 0.05$.

Fig. 1 Inflammatory score and ankle perimeter

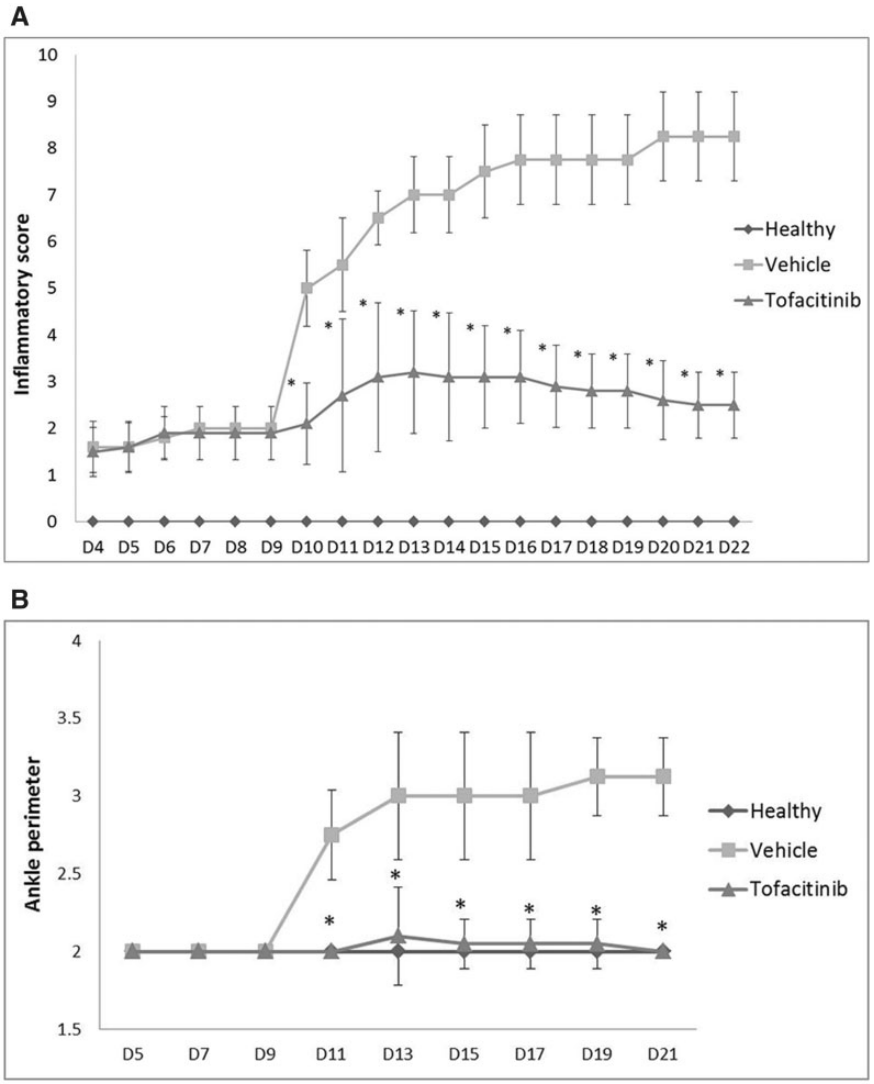

(**A**) Inflammatory score. The tofacitinib group was compared with the vehicle group (arthritic). Results showed statistical differences throughout time from day 10 ($P = 0.0071$) until day 22 ($P = 0.0058$). (**B**) Ankle perimeter. The tofacitinib group was compared with the vehicle group (arthritic). Results showed statistical differences throughout time from day 11 ($P = 0.0057$) until day 22 ($P = 0.0056$). Statistical differences were determined with the non-parametric Mann–Whitney *U*-test using GraphPad Prism (GraphPad, San Diego, CA, USA). Differences were considered statistically significant for $P \leqslant 0.05$. Healthy: n = 20; arthritic: n = 20; tofacitinib: n = 10.

Results

Tofacitinib effectively reduced inflammation in the AIA rat model of arthritis

Results showed that tofacitinib effectively controlled and abrogated disease development in comparison with untreated arthritic rats (Fig.1A). Moreover, untreated arthritic animals sharply increased the ankle perimeter throughout disease progression, which did not occur in tofacitinib-treated animals (Fig.1B).

Tofacitinib abrogated local joint inflammation and local bone and cartilage damage in AIA rats

The sublining layer infiltration (Fig. 2A and B) and the number of lining layer cells (Fig. 2C) were lower in the tofacitinib group when compared with the untreated arthritic group at the end of the study ($P < 0.0001$). Tofacitinib was also effective in preventing joint bone erosions (Fig. 2D) and cartilage damage (Fig. 2E; $P < 0.0001$ and $P = 0.0001$ tofacitinib group *vs* arthritic rats, respectively). Tofacitinib was able to diminish inflammation and local

Fig. 2 Inflammatory and structural score applied to the rat ankle histology

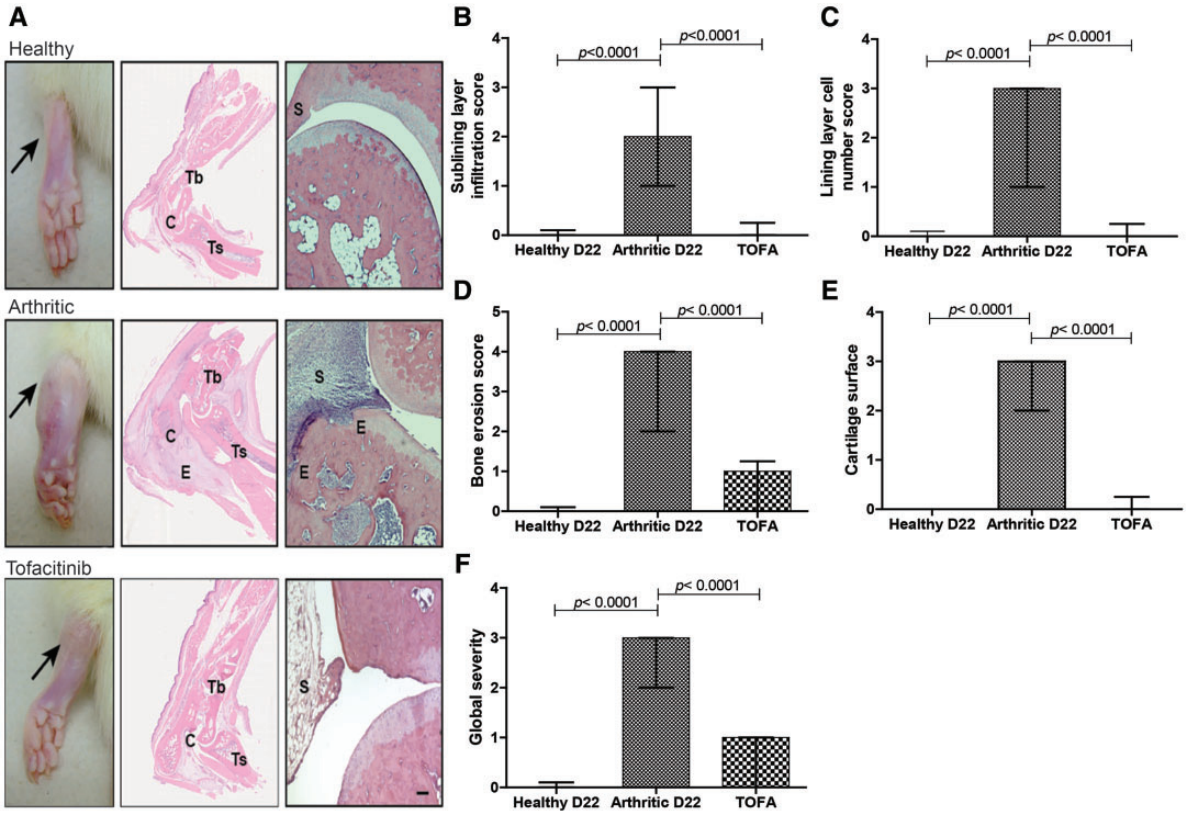

(**A**) Histological images of joints after tofacitinib treatment. These patterns are merely illustrative of the types of histological features observed. Black arrow indicates the absence or presence of ankle swelling in rat hind paws. C: calcaneus; E: erosion or oedema ; S: synovia; Tb: tibia; Ts: tarso. Scale bar: 100 μm. Tofacitinib suppressed inflammation and tissue damage locally in the joints of rats with adjuvant-induced arthritis. A semi-quantitative evaluation of histological sections was performed. Notice that tofacitinib inhibited cellular infiltration (**B**), completely reversed the number of lining layer cells to the normal values (**C**) and prevented the occurrence of bone erosion (**D**), allowing for a normal cartilage (**E**) and joint structure, comparable to that of healthy rats (**F**). Data are expressed as the median with interquartile range. Differences were considered statistically significant for $P < 0.05$, according to the Mann–Whitney *U*-test. Healthy: n = 20; arthritic: n = 20; tofacitinib: n = 10.

bone damage significantly (Fig. 2F; $P < 0.0001$ tofacitinib group *vs* arthritic rats).

In addition, arthritic rats showed increased numbers of osteoblasts in the hind paw ($P = 0.0029$ *vs* healthy controls). Tofacitinib administration significantly lowered the number of osteoblasts to levels similar to those of healthy controls ($P = 0.0035$ *vs* arthritic rats; supplementary Fig. S1, available at *Rheumatology* Online).

Tofacitinib downregulates the JAK–STAT pathway in bone tissue

A significantly decreased expression of STAT1 (supplementary Fig. S2A, available at *Rheumatology* Online) and SOCS1 (supplementary Fig. 2B, available at *Rheumatology* Online) was observed in the bone of AIA rats treated with tofacitinib, in comparison with arthritic untreated rats ($P = 0.0019$ and $P = 0.044$, respectively).

Tofacitinib reduced bone remodelling and inflammatory markers

We observed that both CTX-I (Fig. 3A) and P1NP (Fig. 3B) were significantly increased in the arthritic group in comparison with the healthy control animals ($P < 0.0001$ and $P = 0.0015$, respectively). The tofacitinib group showed decreased values for CTX-I ($P = 0.0002$) and P1NP ($P = 0.0018$) when compared with the arthritic group (Fig. 3).

RANKL levels were decreased in the serum of tofacitinib-treated rats in comparison with healthy control and untreated arthritic rats ($P = 0.0083$ and $P = 0.0141$, respectively), as observed in Fig 3C. OPG levels were also reduced in the tofacitinib group in comparison with healthy controls and untreated arthritic rats ($P = 0.0031$ and $P = 0.0002$, respectively; Fig. 3D). No differences were observed in the RANKL/OPG ratio between the

Fig. 3 Quantification of bone turnover markers and systemic cytokines

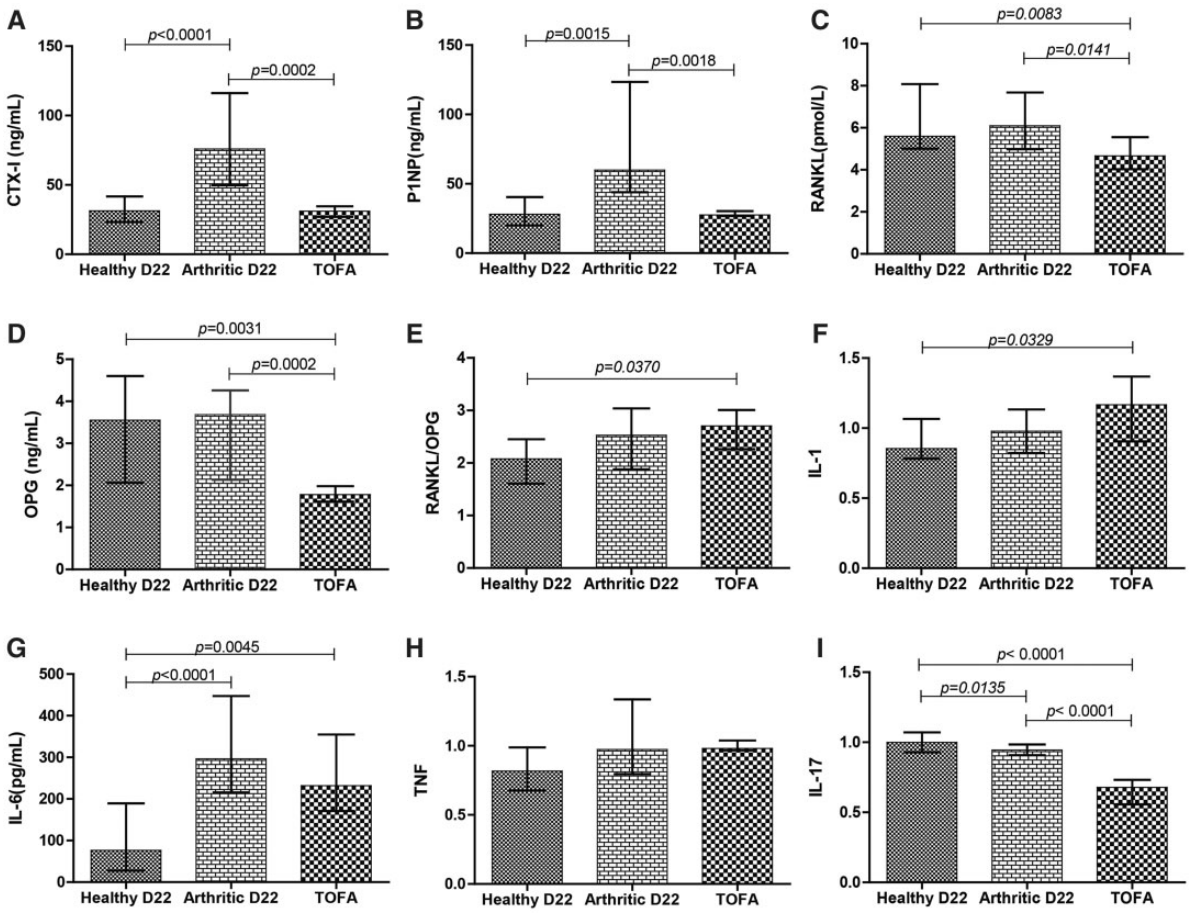

Serum samples collected at day 22 (sacrifice) were analysed by ELISA technique. A bone resorption marker, carboxy-terminal telopeptide of type I collagen (**A**), and bone formation markers, procollagen type I propeptides (**B**), were increased in arthritic rats ($P < 0.0001$ and $P = 0.0015$, respectively). The tofacitinib group showed decreased values for carboxy-terminal telopeptide of type I collagen ($P = 0.0002$) and procollagen type I propeptides ($P = 0.0018$). RANK ligand (**C**) and osteoprotegerin (**D**) were diminished in tofacitinib-treated rats when compared with arthritic untreated group ($P = 0.0141$ and $P = 0.0002$, respectively). The RANK ligand/osteoprotegerin ratio (**E**) showed higher values when compared with the healthy group ($P = 0.0370$). Tofacitinib, in this animal model, did not affect circulating concentrations of IL-1β (**F**) and TNF (**H**). The results also demonstrated a significant decrease in the serum quantification of IL-17 (**I**; $P < 0.0001$) and a tendency towards a decrease of IL-6 (**G**). IL-1, TNF and IL-17 were normalized. Differences were considered statistically significant for $P < 0.05$, according to the Mann–Whitney *U*-test. Healthy: n = 20; arthritic: n = 20; tofacitinib: n = 10.

tofacitinib and arthritic untreated groups. The tofacitinib group showed an increased RANKL/OPG ratio when compared with the healthy control group ($P = 0.0370$; Fig. 3E).

We also quantified the circulating concentrations of IL-1β, IL-6 and TNF, but no differences were found when comparing arthritic rats with animals treated with tofacitinib (Fig. 3F–H). However, there was a slight tendency for IL-6 to be diminished in the tofacitinib group when compared with untreated arthritic animals.

Tofacitinib administration significantly reduced the levels of IL-17 detected in peripheral blood ($P < 0.0001$, tofacitinib group *vs* untreated arthritic rats after 22 days of disease induction; Fig. 3I).

Micro-CT

Arthritic rats showed a reduction in cortical bone cross-sectional area (Fig. 4A) and thickness (Fig. 4B), and tofacitinib treatment did not restore these cortical changes ($P < 0.0001$ *vs* healthy controls, respectively). These bone changes affected the torsion capability of the bone, as shown by decreased values of the polar moment of inertia (Fig. 4C) in the arthritic and tofacitinib groups ($P = 0.0059$ and $P = 0.0197$ *vs* healthy controls,

Fig. 4 Micro-CT analysis of samples of rat tibia

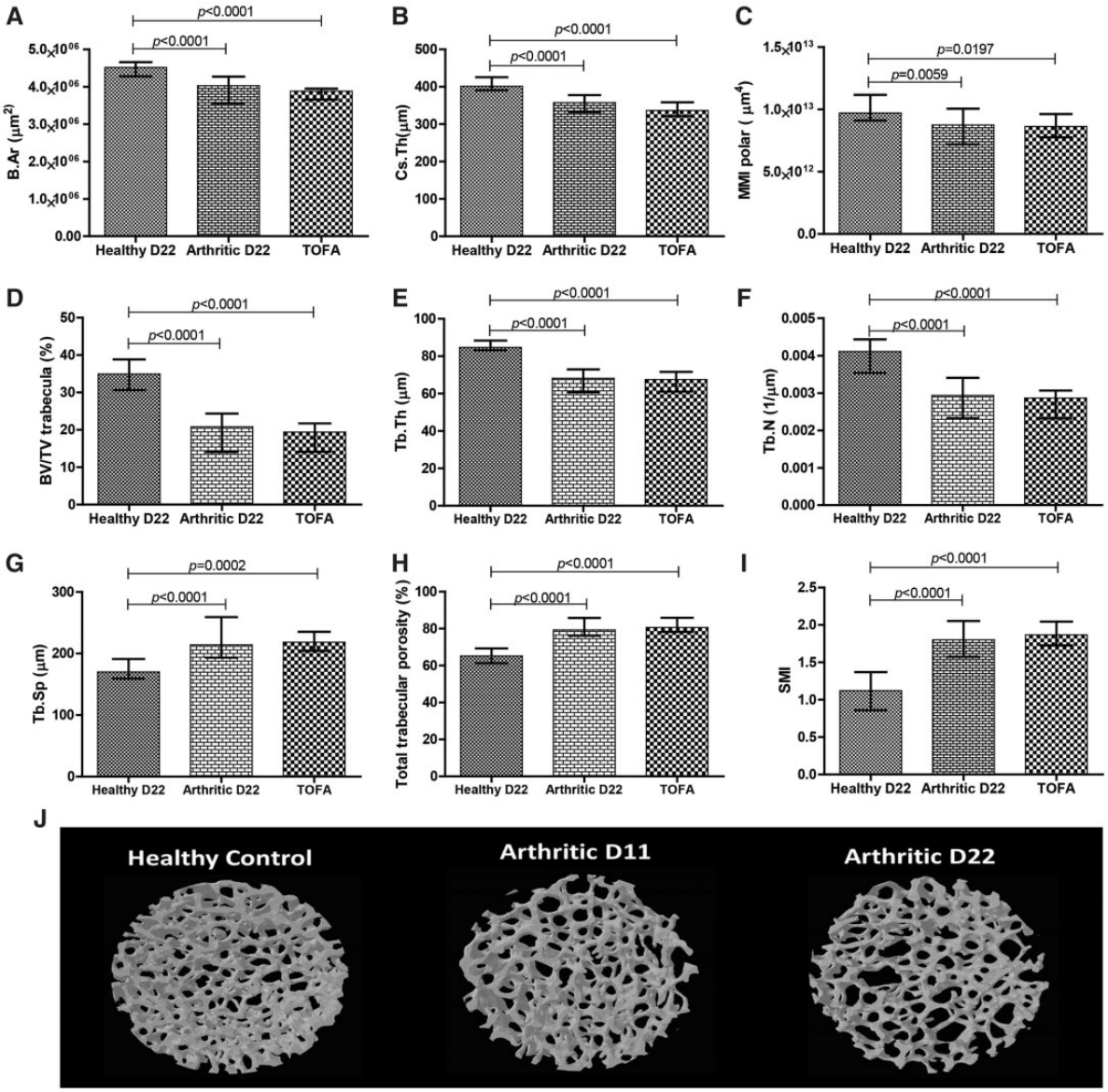

The arthritic and tofacitinib groups showed decreased values for cortical cross-sectional bone area (**A**), thickness (**B**) and polar moment of inertia (**C**) when compared with healthy controls. Trabecular bone also showed lower values of ratio bone volume/tissue volume (**D**), trabecular thickness (**E**) and number (**F**) in comparison with healthy controls. Arthritic and tofacitinib rats demonstrated higher values of trabecular separation (**G**) and porosity (**H**) when compared with healthy controls. The structural model index showed decreased values in arthritic and tofacitinib rats compared with healthy rats. Micro-CT images from tibias of healthy, arthritic untreated and tofacitinib groups (**J**). Images were acquired with SkyScan 1272 (Bruker microCT, Kontich, Belgium). Differences were considered statistically significant for $P < 0.05$, according to the Mann–Whitney *U*-test. Healthy: n = 20; arthritic: n = 20; tofacitinib: n = 10.

respectively). Trabecular bone also presented deterioration with arthritis, as evidenced by a reduced trabecular bone volume fraction (Fig. 4D; $P = 0.0007$ and $P < 0.0001$ *vs* healthy controls, respectively), thickness (Fig. 4E) and number (Fig. 4F; $P < 0.0001$ *vs* healthy controls) and also by an increased trabecular separation (Fig. 4G; $P < 0.0001$ in arthritic group and $P = 0.0002$ in tofacitinib group *vs* healthy controls) and porosity (Fig. 4H; $P < 0.0001$ *vs* healthy controls). Furthermore, the structure model index (Fig. 4I) showed reduced values in the arthritic and tofacitinib groups ($P < 0.0001$ *vs* healthy controls, respectively).

FIG. 5 Bone mechanical properties assessed by three-point bending tests in rat femur

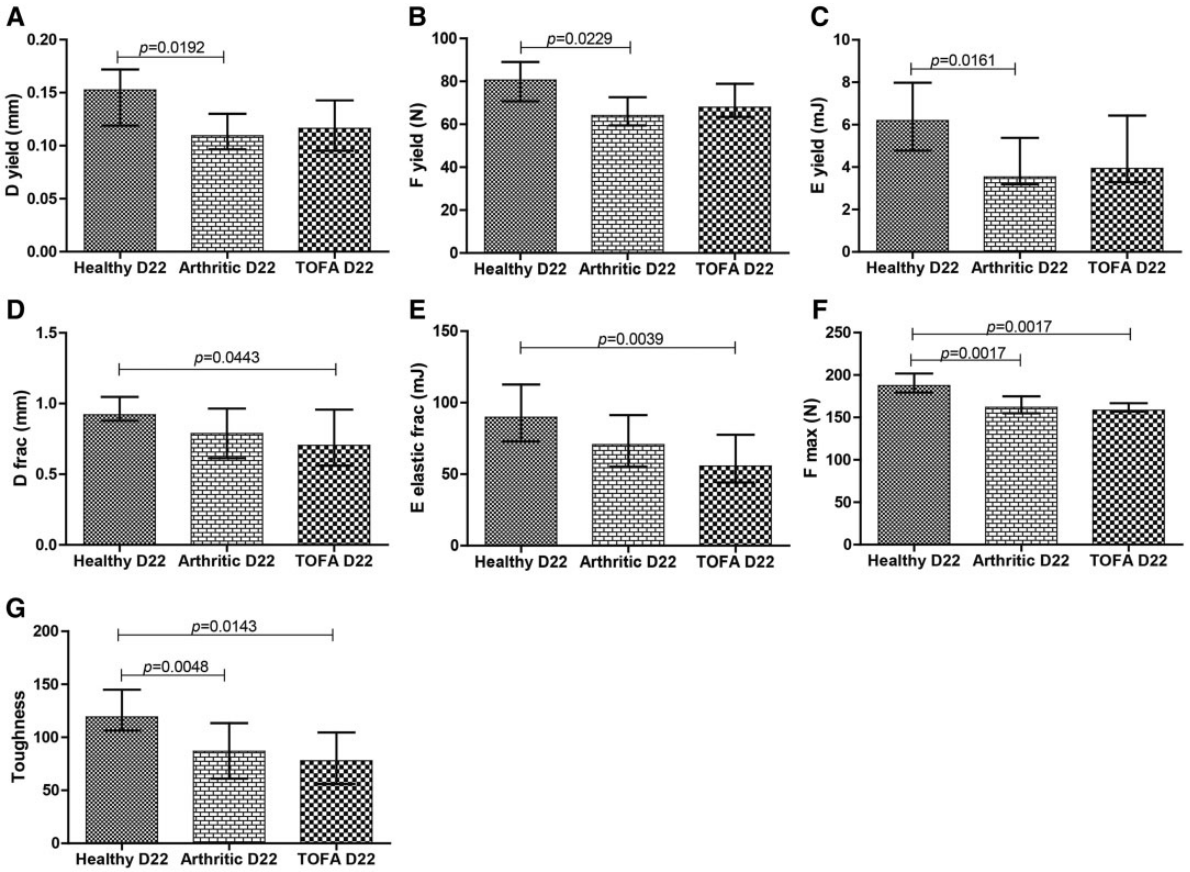

Results showed that arthritic rats have decreased properties at the yield point, related to displacement (**A**), strength (**B**) and pre-yield energy (elastic energy; **C**). Tofacitinib-treated rats had a significant decrease in displacement (**D**) and elastic properties (**E**) at the fracture point. Arthritic and tofacitinib-treated bones required a lower maximal load (**F**) to fracture, and a decreased toughness (**G**) was observed. Differences were considered statistically significant for $P < 0.05$, according to the Mann–Whitney *U*-test. Healthy: n = 20; arthritic: n = 20; tofacitinib: n = 10.

Tofacitinib could not rescue trabecular bone integrity and trabecular bone properties in treated rats (Fig. 4J).

Three-point bending

As shown in Fig. 5, arthritic rats revealed decreased mechanical properties at the yield point, namely displacement (P = 0.0192 *vs* healthy controls; Fig. 5A), strength (P = 0.0229 *vs* healthy control; Fig. 5B) and pre-yield energy (elastic energy; P = 0.0161 *vs* healthy controls; Fig. 5C). Tofacitinib-treated rats showed a significantly decreased displacement (P = 0.0039 *vs* healthy controls; Fig. 5D) and elastic properties (P = 0.0443 *vs* healthy controls; Fig. 5E) at the fracture point. The results also demonstrated that arthritic and tofacitinib-treated rats had decreased maximal load (P = 0.0017 *vs* healthy controls; Fig. 5F). Finally, arthritic rats and the tofacitinib-treated group showed a significant decrease in toughness (P = 0.0143 and P = 0.0048 *vs* healthy controls, respectively; Fig. 5G).

Tofacitinib increased bone hardness

Arthritic rats had decreased hardness in cortical (Fig. 6A) and trabecular bone (Fig. 6B; P = 0.0010 and P = 0.0080 in arthritic rats *vs* healthy controls, respectively). In contrast, rats treated with tofacitinib showed restored hardness in cortical bone (Fig. 6A) and increased hardness in trabecular bone (Fig. 6B; P = 0.0003 and P = 0.0012 *vs* untreated arthritic rats, respectively). No differences were observed in the other parameters analysed.

Concentric lamellae in secondary osteons (SO) were identified more frequently in arthritic animals (Fig. 6F) than in healthy controls (P = 0.0022) and tofacitinib-treated animals (P = 0.0043; Fig. 6C). On the contrary, healthy animals (Fig. 6E) and tofacitinib-treated animals (Fig. 6G) presented more PL structures than concentric lamellae.

In addition, arthritic animals showed an increased area occupied by osteocyte lacunae in the total tissue, when compared with healthy and tofacitinib-treated animals (Fig. 6D; P = 0.0067 and P = 0.0011, respectively).

Fig. 6 Bone mechanical properties assessed by nanoindentation and respective topographic images

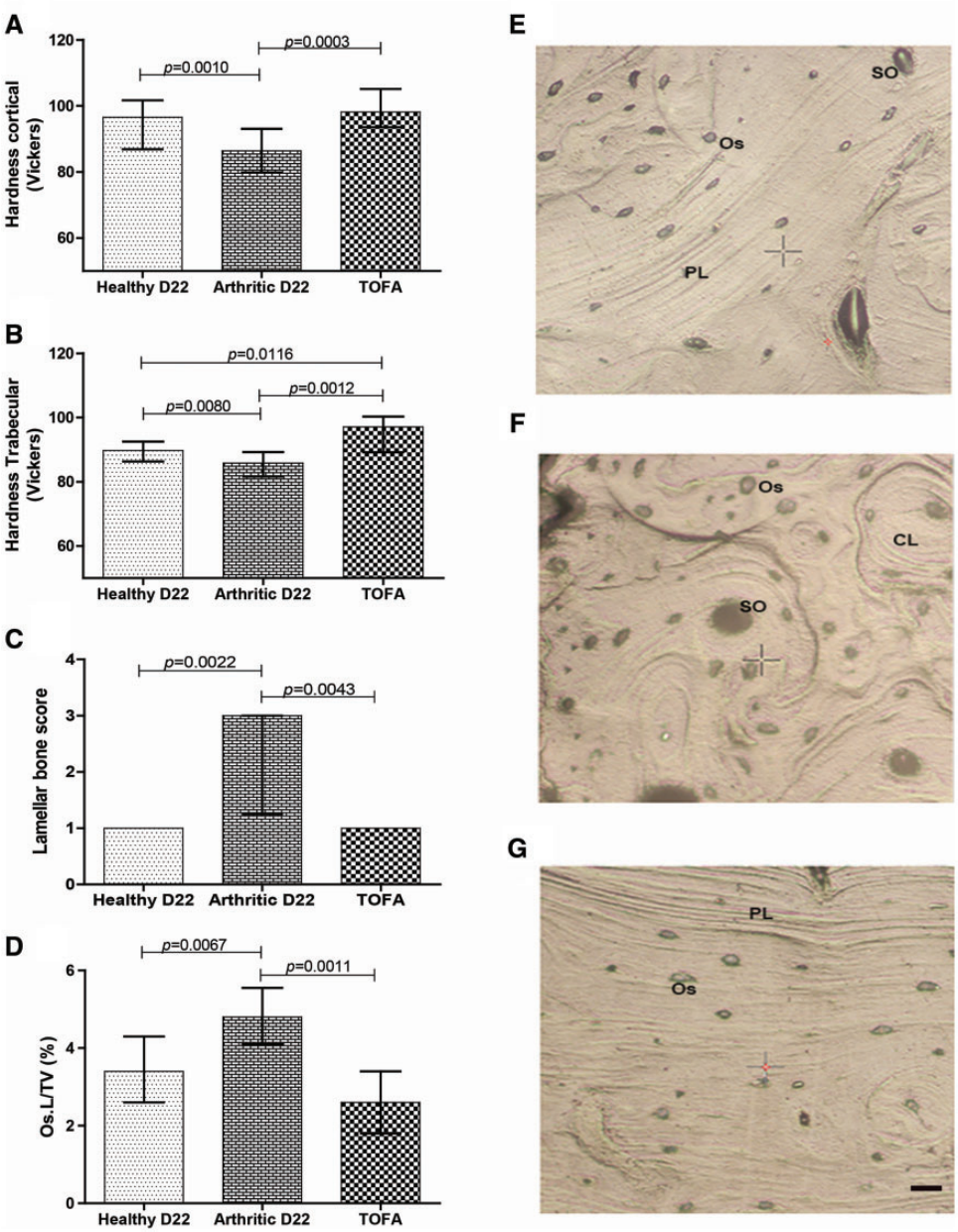

Nano-mechanical tests revealed a decreased cortical (**A**) and trabecular (**B**) hardness in the arthritic group at day 22 when compared with healthy rats. Of note, rats treated with tofacitinib showed increased hardness in the cortical (**A**) and trabecular (**B**) bone in comparison with untreated arthritic rats. Results demonstrated that the number of concentric lamellae (**C**) and ratio of area occupied by osteocyte lacunae in the total tissue (**D**) were higher when compared with the healthy control and tofacitinib-treated groups at day 22. Images are merely illustrative of the types of histological features observed. Concentric lamellae were identified in SO, characteristic of arthritic animals (**F**). On the contrary, PL were identified in the healthy control (**E**) and tofacitinib-treated groups (**G**). Scale bar: 20 μm. Differences were considered statistically significant for $P < 0.05$, according to the Mann–Whitney U-test. Healthy: n = 20; arthritic: n = 20; tofacitinib: n = 10. CL: concentric lamellae; Os: osteocytes; PL: parallel lamellae; SO: secondary osteons.

Discussion

In this study, we showed that tofacitinib in the AIA rat model abrogated synovitis and prevented joint destruction. This was paralleled by decreased levels of IL-17, IL-6, RANKL and OPG and by a reduced bone turnover in tofacitinib-treated animals. Despite preserving bone cortical and trabecular hardness, tofacitinib did not

revert the effects of arthritis on cortical and trabecular bone structure and on mechanical properties.

These results are in line with the pre-clinical and clinical evidence regarding the efficacy of tofacitinib in controlling clinical manifestations of RA and preventing joint damage [11, 25–29]. However, the effects of tofacitinib on the systemic bone fragility of patients affected by RA are still unknown, and thus, the results of this exploratory animal study can contribute to a better understanding of the effect on bone of JAK–STAT inhibition.

At the tissue level, measured by nanoindentation, tofacitinib treatment conserved bone hardness (or even increased in the case of the trabecular component). We also observed, at days 11 and 22 after induction of arthritis, concentric lamellae in SO microstructures resulting from high bone remodelling, as previously described [15, 30, 31]. Dall'Ara *et al.* [31] suggested that larger numbers of these younger, less mineralized and less hard structures could be related to reduced hardness of bone tissue identified by nanoindentation. On the contrary, healthy and tofacitinib-treated animals presented more PL structures than concentric lamellae in SO structures, PL structures which represents the mature bone structure (and normal bone remodelling) are 10% harder than the concentric lamella structure. [31]. In addition, arthritic animals had an increased area occupied by osteocyte lacunae in the total tissue. Tofacitinib-treated animals, in contrast, had a normal number of osteocyte lacunae and of the lacunar area per tissue volume. Osteocytes are responsible for the maintenance of bone homeostasis, regulating the behaviour of osteoblasts and osteoclasts by communicating through gap junctions [32]. Studies have revealed that osteocytes from OA patients have an irregular morphology, with limited ability to respond to mechanical stimuli, leading to significant changes in the structure and mineral density [33]. Despite still being unclear, this apparent change of osteocyte morphology in arthritic bone might contribute to the nanomechanical changes observed in this context.

Micro-CT and three-point bending tests revealed that tofacitinib did not revert the effects of arthritis on cortical and trabecular bone structure and mechanical properties. There are several possible explanations for these observations. Using the same animal model, we were able to revert the structural and mechanical damage induced by arthritis using an experimental compound [18]. However, the kinetics of the effects of tofacitinib might be different, needing more exposure time to have an impact on bone quality. The effect at a tissue level might be an early sign of its delayed impact on bone. Of interest, an increase in hardness is associated with a decrease in the relative ratio of elastic-to-plastic behaviour of the tissue, and thus, it is unclear whether it ultimately represents a true improvement in mechanical properties. Another explanation might be related to the mechanism of action. Tofacitinib targets JAK1 and JAK3, downregulating STAT1 and STAT3 of the JAK–STAT signalling pathway [11, 12, 25], and these intracellular molecules have complex interactions with bone. JAK1 is expressed in bone cells and is involved in bone formation. The depletion of JAK1 promotes a delay in bone growth, suggesting that JAK1 is crucial for skeletal development. In contrast, in osteoblasts STAT1 inhibits transcription of *Runx2*, the master transcription factor of osteoblast differentiation. Thus, STAT1 is an inhibitor of differentiation of osteoblasts, and the inactivation of STAT1 leads to an osteopetrotic bone phenotype [34]. Consistent with the higher bone mass in STAT1-deficient mice, inactivation of STAT1 can accelerate fracture repair [35]. These data suggest that STAT1 negatively regulates bone formation *in vivo* [36]. On the contrary, the JAK–STAT3 signal transduction pathway promotes osteoblast differentiation [36]. In fact, inactivation of STAT3 in osteoblasts leads to lower bone mass attributable to inhibition of bone formation, and *STAT3* mutations increase osteoclast number and bone resorption and are associated with recurrent fractures. It is conceivable that these types of molecular interactions with bone have an overall effect that might not be totally compensated by the benefits obtained by the control of inflammation.

Broad, unspecific molecular effects of MTX potentiate the effect of targeted therapies. This is expected to occur in the combination of MTX with tofacitinib and might contribute, as already explored in clinical trials, to an increment in inflammatory control, probably fully compensating bone damage [37]. To clarify these open questions it will be relevant to test several doses of tofacitinib and also combination therapy with MTX, in longer duration arthritis models and in healthy animals. In addition, the discrepancy between the effect of tofacitinib on joint erosions and on skeletal bone deserves a full microstructural study of intra-articular bone compared with skeletal bone.

Funding: This work was supported by Aspire 2013 prize from Pfizer. The funders had no role in study design, data collection and analysis, decision to publish or preparation of the manuscript.

Disclosure statement: J.E.F. participated in advisory boards, received research grants and acted as a Speaker for Pfizer, Lilly, Merck Sharp & Dohme, Union chimique belge, Abbvie, Bristol-Myers Squibb, Roche, Biogen and Hospira. All other authors have declared no conflicts of interest.

Supplementary data

Supplementary data are available at *Rheumatology* Online.

References

1 Alamanos Y, Drosos AA. Epidemiology of adult rheumatoid arthritis. Autoimmun Rev 2005;4:130–6.

2 Fonseca JE, Cortez-Dias N, Francisco A *et al*. Inflammatory cell infiltrate and RANKL/OPG expression in rheumatoid synovium: comparison with other inflammatory arthropathies and correlation with outcome. Clin Exp Rheumatol 2005;23:185–92.

3 Boyle WJ, Simonet WS, Lacey DL. Osteoclast differentiation and activation. Nature 2003;423:337–42.

4 Moura RA, Cascao R, Perpetuo I *et al*. Cytokine pattern in very early rheumatoid arthritis favours B-cell activation and survival. Rheumatology 2011;50:278–82.

5 Cascao R, Moura RA, Perpétuo I *et al*. Identification of a cytokine network sustaining neutrophil and Th17 activation in untreated early rheumatoid arthritis. Arthritis Res Ther 2010;12:R196.

6 Caetano-Lopes J, Canhão H, Fonseca JE. Osteoimmunology — the hidden immune regulation of bone. Autoimmun Rev 2009;8:250–5.

7 Caetano-Lopes J, Rodrigues A, Lopes A *et al*. Rheumatoid arthritis bone fragility is associated with upregulation of IL17 and DKK1 gene expression. Clin Rev Allergy Immunol 2014;47:38–45.

8 Marshall D, Johnell O, Wedel H. Meta-analysis of how well measures of bone mineral density predict occurrence of osteoporotic fractures. BMJ 1996;312:1254–9.

9 Kroot E, Laan R. Bone mass in rheumatoid arthritis. Clin Exp Rheum 2000;18(5; SUPP/21):S-12.

10 Tofacitinib. Drugs R D 2010;10:271–84.

11 Meyer DM, Jesson MI, Li X *et al*. Anti-inflammatory activity and neutrophil reductions mediated by the JAK1/JAK3 inhibitor, CP-690,550, in rat adjuvant-induced arthritis. J Inflamm 2010;7:41.

12 Maeshima K, Yamaoka K, Kubo S *et al*. The JAK inhibitor tofacitinib regulates synovitis through inhibition of interferon-γ and interleukin-17 production by human CD4+ T cells. Arthritis Rheum 2012;64:1790–8.

13 European Medicines Agency. Eight medicines recommended for approval, including two biosimilars. 2017 http://www.ema.europa.eu/ema/index.jsp?curl=pages/news_and_events/news/2017/01/news_detail_002682.jsp&mid=WC0b01ac058004d5c1 (May 2017, date last accessed).

14 Faul F, Erdfelder E, Lang AG, Buchner A. G*Power 3: a flexible statistical power analysis program for the social, behavioral, and biomedical sciences. Behav Res Methods 2007;39:175–91.

15 Vidal B, Cascão R, Vale AC *et al*. Arthritis induces early bone high turnover, structural degradation and mechanical weakness. PLoS One 2015;10:e0117100.

16 Ellis PD. Effect size calculators. 2009. http://mywebpolyueduhk/mspaul/calculator/calculatorhtml (May 2017, date last accessed).

17 Schopf LR, Anderson K, Jaffee BD. Rat models of arthritis: Similarities, differences, advantages, and disadvantages in the identification of novel therapeutics; 2006: pp. 1–34. In: Stevenson CS Marshall LA, Morgan DW, eds. In vivo Models of Inflammation, 2nd ed. Berlin: Birkhauser Verlag.

18 Cascão R, Vidal B, Raquel H *et al*. Effective treatment of rat adjuvant-induced arthritis by celastrol. Autoimmun Rev 2012;11:856–62.

19 Chen DL, Wang DS, Wu WJ *et al*. Overexpression of paxillin induced by miR-137 suppression promotes tumor progression and metastasis in colorectal cancer. Carcinogenesis 2013;34:803–11.

20 Bouxsein ML, Boyd SK, Christiansen BA *et al*. Guidelines for assessment of bone microstructure in rodents using micro-computed tomography. J Bone Miner Res 2010;25:1468–86.

21 Herlin M, Finnilä MA, Zioupos P *et al*. New insights to the role of aryl hydrocarbon receptor in bone phenotype and in dioxin-induced modulation of bone microarchitecture and material properties. Toxicol Appl Pharmacol 2013;273:219–26.

22 Zhang R, Gong H, Zhu D *et al*. Multi-level femoral morphology and mechanical properties of rats of different ages. Bone 2015;76:76–87.

23 Oliver WC, Pharr GM. An improved technique for determining hardness and elastic modulus using load and displacement sensing indentation experiments. J Mater Res 1992;7:1564–83.

24 Parfitt AM, Drezner MK, Glorieux FH *et al*. Bone histomorphometry: standardization of nomenclature, symbols, and units. Report of the ASBMR Histomorphometry Nomenclature Committee. J Bone Miner Res 1987;2:595–610.

25 LaBranche TP, Jesson MI, Radi ZA *et al*. JAK inhibition with tofacitinib suppresses arthritic joint structural damage through decreased RANKL production. Arthritis Rheum 2012;64:3531–42.

26 Milici AJ, Kudlacz EM, Audoly L, Zwillich S, Changelian P. Cartilage preservation by inhibition of Janus kinase 3 in two rodent models of rheumatoid arthritis. Arthritis Res Ther 2008;10:R14.

27 Tanaka Y, Maeshima K, Yamaoka K. In vitro and in vivo analysis of a JAK inhibitor in rheumatoid arthritis. Ann Rheum Dis 2012;71 (Suppl 2):i70–4.

28 Tanaka Y, Yamaoka K. JAK inhibitor tofacitinib for treating rheumatoid arthritis: from basic to clinical. Mod Rheumatol 2013;23:415–24.

29 Lee EB, Fleischmann R, Hall S *et al*. Tofacitinib versus methotrexate in rheumatoid arthritis. New Engl J Med 2014;370:2377–86.

30 Bailey AJ, Mansell JP, Sims TJ, Banse X. Biochemical and mechanical properties of subchondral bone in osteoarthritis. Biorheology 2004;41:349–58.

31 Dall'Ara E, Ohman C, Baleani M, Viceconti M. Reduced tissue hardness of trabecular bone is associated with severe osteoarthritis. J Biomechanics 2011;44:1593–8.

32 Taylor AF, Saunders MM, Shingle DL *et al*. Mechanically stimulated osteocytes regulate osteoblastic activity via gap junctions. Am J Physiol Cell Physiol 2007;292:C545–52.

33 Jaiprakash A, Prasadam I, Feng JQ *et al*. Phenotypic characterization of osteoarthritic osteocytes from the sclerotic zones: a possible pathological role in subchondral bone sclerosis. Int J Biol Sci 2012;8:406–17.

34 Kim S, Koga T, Isobe M *et al*. Stat1 functions as a cytoplasmic attenuator of Runx2 in the transcriptional program of osteoblast differentiation. Genes Dev 2003;17:1979–91.

35 Tajima K, Takaishi H, Takito J *et al*. Inhibition of STAT1 accelerates bone fracture healing. J Orthop Res 2010;28:937–41.

36 Li J. JAK-STAT and bone metabolism. JAKSTAT 2013;2:e23930.

37 van der Heijde D, Tanaka Y, Fleischmann R *et al*. Tofacitinib (CP-690,550) in patients with rheumatoid arthritis receiving methotrexate: twelve-month data from a twenty-four-month phase III randomized radiographic study. Arthritis Rheum 2013;65:559–70.